IEEE Transactions on Industrial Electronics, no., pp. 1–1, 2018

Input-Admittance Passivity Compliance for Grid-Connected Converters with LCL Filter

E. R. Diaz, F. D. Freijedo, J. M. Guerrero, *et al.*

POWER ELECTRONICS LABORATORY
ÉCOLE POLYTECHNIQUE FÉDÉRALE DE LAUSANNE

This article has been accepted for publication in a future issue of this journal, but has not been fully edited. Content may change prior to final publication. Citation information: DOI 10.1109/TIE.2018.2835374, IEEE Transactions on Industrial Electronics

Input-Admittance Passivity Compliance for Grid-Connected Converters with LCL Filter

Enrique Rodriguez-Diaz, *Member, IEEE*, Francisco D. Freijedo, *Senior Member, IEEE*, Josep M. Guerrero, *Fellow Member, IEEE*, Juan-Alberto Marrero-Sosa, and Drazen Dujic, *Senior Member, IEEE*

***Abstract*—This work presents a design methodology and its experimental validation for the input-admittance passivity compliance of LCL grid-connected converters. The designs of the LCL filter parameters and discrete controller are addressed systematically, and suitable design guidelines are provided. The controller design is developed in the z-domain, with capacitor voltage based active damping used as degree of freedom to compensate for system delay effects. The role of resistive components in the circuit, which have inherent dissipative properties, is also discussed. As an outcome of the design, a passive input admittance shaping is obtained. The theoretical development is further verified in a low-scale prototype supplied from a controllable grid simulator. For the sake of generality, different combinations of resonant to sampling frequency are tested. Experimental results fully prove the input-admittance passivity compliance.**

***Index Terms*—Admittance measurement, current control, pulse width modulation converters, stability criteria.**

I. Introduction

Stability of grid-tied voltage source converters (VSCs) connected to highly variable grid conditions is a challenging issue. This is the case of traction applications, in which the electric circuit seen by the locomotive converter (i.e., the plant) is continuously changing during operation [1], [2]. Looking at renewable energy applications, high uncertainty in the plant model is found in large wind farms due to elements such as long cables, capacitor banks and transformers [3]–[5].

Classical closed-loop control theory approaches face important difficulties to deal with uncertainties of the plant (i.e., the electric circuit at which the VSC is connected). Alternatively, the input-admittance criterion successfully deals with a limited knowledge of physical environment, since it provides a sufficient condition for stability [6]. Input-admittance passivity compliance is a requirement in traction standards [1], [2], [7]. More recently, the interest on design for passivity methodologies for grid-connected VSCs has grown owing to the drastical increase of power electronics in renewable energy applications [8]–[11].

Design for passivity methodologies, particularized for grid-connected VSCs, can be summarized as follows:

i) the closed loop control problem is expressed in terms of the impedance stability criterion [6], [8].
ii) the environment model is unknown, but it is assumed to be passive. Defining $Z_g(\omega)$ as a grid impedance that defines the environment dynamics, $\mathrm{Re}\{Z_g(\omega)\} > 0$, or equivalently $|\angle Z_g(\omega)| \leq \pi/2\,\mathrm{rad}$, define the condition for passivity.
iii) subsequently, stability is assured if the VSC input-admittance, defined as $Y_g(\omega)$, is also passive; i.e., the VSC control and hardware designs should focus on a $Y_g(\omega)$ shaping, such that $\mathrm{Re}\{Y_g(\omega)\} > 0$ (i.e., $|\angle Y_g(\omega)| \leq \pi/2\,\mathrm{rad}$).

Systematic procedures to set control filters and parameters is provided with the goal of shaping the converter admittance to be passive [8]–[11]. However, even though a comprehensive work is identified in the recent state of the art, some open problems could be still identified:

i) usually, the controller analyses are developed in the continous domain [9], [11], which may imply some discrepancies with discrete implementation. Alternative, a controller in the discrete domain can be employed for the calculation of the controller gains [10].
ii) The criterion to set a high frequency limit for the controller design is not clear. In principle, the Nyquist frequency is considered [8], [9], but the role of alias terms on the stability have been also discussed recently [12]. However, the VSC control action effectiveness is reduced to a relatively low frequency range of the spectrum [13], [14].
iii) Most of the design for passivity efforts are focused on the controller design, but the role of natural damping of the system is usually overlooked.

In relation to the last two points, the LCL interface filter has been suggested as a convenient structure to provide input-admittance passivity compliance [10], which in principle may seem contradictory: LCL filters are placed in order to attenuate switching harmonics, but, as a side effect, they introduce a resonance into the plant, which may compromise the VSC stability [15]–[20]. An intuitive physical explanation for the good stability properties given by the LCL filter is the fact that the capacitor branch, which is in parallel to the VSC one, absorbs most of the high frequency components from the grid;

Manuscript received November 21, 2017; revised March 28, 2018; accepted April 29, 2018.

This work was supported in part by the Swiss Federal Office of Energy under the Granted Project "Medium-Voltage Direct-Current Energy Conversion Technologies and Systems (SI/501259)".

Enrique Rodriguez-Diaz and Josep M. Guerrero are with the Department of Energy Technology, AAU, 9220 Aalborg East, Denmark. E-mails: erd@et.aau.dk and joz@et.aau.dk.

Francisco D. Freijedo (corresponding author) and Drazen Dujic are with the Power Electronics Laboratory, EPFL, CH1005, Lausanne, Switzerland. E-mails: francisco.freijedo@epfl.ch (Tel: +41 21 693 47 89 and Fax: +41 21 693 26 00) and drazen.dujic@epfl.ch.

Juan-Alberto Marrero-Sosa is with ABB Traction, CH5300, Turgi, Switzerland. E-mail:juan-alberto.marrero-sosa@ch.abb.com.

This article has been accepted for publication in a future issue of this journal, but has not been fully edited. Content may change prior to final publication. Citation information: DOI 10.1109/TIE.2018.2835374, IEEE Transactions on Industrial Electronics

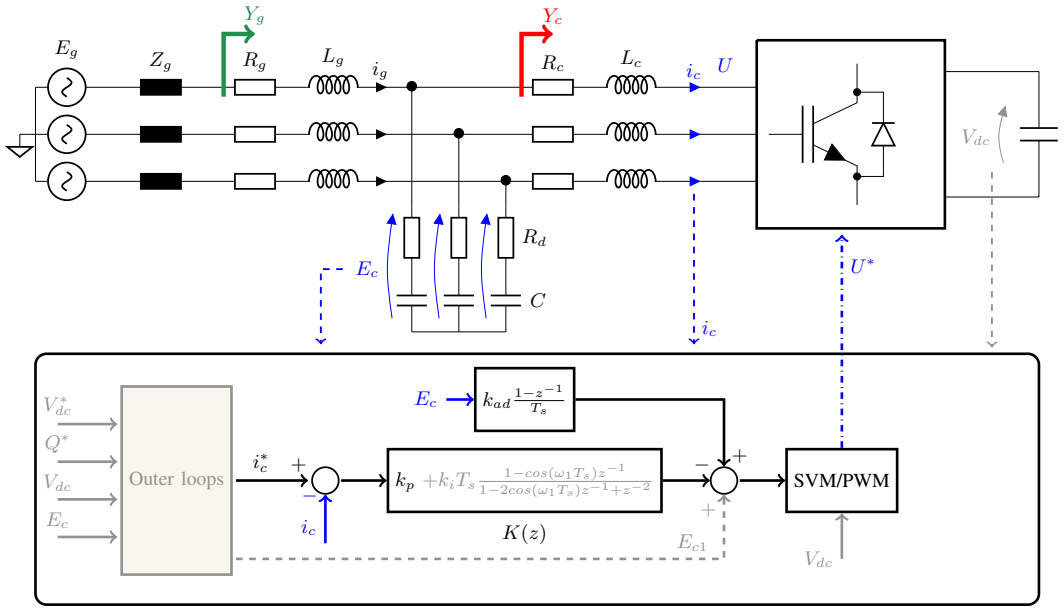

Fig. 1. LCL grid-connected converter with current control including a capacitor voltage based active damping.

therefore, the closed-loop control action is hardly affected by high order harmonics perturbations in the grid side.

This work deepens on the input-admittance passivity compliance considering the beneficial impact of the LCL filter. With regard to the previous study in [10], two major contributions are provided, say i) systematic guidelines for control and hardware design are provided; ii) a comprehensive set of experimental tests based on the EN50388 standard [7] is provided, which fully prove the main theoretical hypotheses.

The rest of the paper is organized as follows. Section II shows an overall description of a LCL grid-connected converter and its discrete current controller. Section III presents the core hypotheses and design guidelines to achieve an input-admittance passivity compliant system. Section IV details the experimental verification test-bed and includes figures of merit to prove the input-admittance compliance. Finally, the main conclusions of this work are summarized.

II. System Description and Problem Formulation

Fig. 1 represents a LCL grid-connected VSC working in current control mode. The voltages E_g, E_c and U represent the stiff grid, point of connection and VSC voltages, respectively. The LCL output filter is formed by the converter side inductance, a capacitive branch and grid side inductance, presumably a transformer leakage model [4], [19], [20]. The converter side inductive filter is defined by series inductance L_c and resistance R_c. The capacitance is given by a parallel capacitance C in series with a damping resistor R_d; R_d can be considered a degree of freedom to physically increase the damping of the LCL filter [16]. The secondary inductance is given by L_g with R_g in series. The grid model is represented by the grid impedance Z_g. It depends on power system circuit and grid conditions [3], [5], but for input-admittance passivity compliance is assumed to be a passive environment.

A. Controller

Fig. 1 includes the current loop. $\mathbf{K}(z)$ represents the main controller. A proportional resonant (PR) controller implemented in $\alpha\beta$-frame is considered in this work:

$$\mathbf{K}(z) = (k_p + k_i T_s \frac{1 - cos(\omega_1 T_s) z^{-1}}{1 - 2cos(\omega_1 T_s) z^{-1} + z^{-2}})\mathbf{I} \quad (1)$$

with k_p and k_i being the proportional and resonant gains, ω_1 the fundamental frequency and $T_s = 2\pi/\omega_s$ the controller sampling period, respectively. The resonant filter transfer function corresponds to the impulse-invariant method [21]. $\mathbf{I}$ is a 2x2 unity matrix, that means that $\mathbf{K}(z)$ is diagonal [20].

The control action calculation also includes an $\mathbf{E}_c$ voltage feedforward double path, with the following objectives: i) provide a filtered value of the main grid component to improve the initial transient [8] and ii) an active damping action based on capacitor voltage derivative term [9], [15]. The active damping action using a backward-Euler discretization is

$$\mathbf{F}(z) = (k_{ad} \frac{1 - z^{-1}}{T_s})\mathbf{I}. \quad (2)$$

with k_{ad} being the active damping gain [15]. $\mathbf{F}(z)$ is also a diagonal matrix defined in the $\alpha\beta$-frame.

A matrix notation has been employed until now in order to differentiate three-phase signals and scalar variables. Subsequently, for the sake of generality scalar notation is used, as no couplings between phases are considered. This assumption is accurate for $\alpha\beta$-frame, as both the controller and physical signal are defined diagonal [20], [22].

B. LCL filter

In most grid-connected applications, the hardware design is imposed by the transformer leakage inductance, which sets L_g [19], [23]. Typical values for the secondary inductance are

This article has been accepted for publication in a future issue of this journal, but has not been fully edited. Content may change prior to final publication. Citation information: DOI 10.1109/TIE.2018.2835374, IEEE Transactions on Industrial Electronics

then in the range $[0.06, 0.1]$ p.u. (wind turbine rated power is used for base calculations) [19]. Following LCL design basic guidelines, the secondary inductance also constraints the selection of the converter filter: a primary inductance equal to the transformer inductance is a reasonable design to optimize the switching harmonics filtering [15], [19], [20]. Using L_g as a constraint, in practice, the main degree of freedom of the LCL filter is the choice of the capacitance C. The rated LCL resonance frequency (angular) is

$$\omega_{res} = \sqrt{\frac{L_c + L_g}{L_c L_g C}}. \tag{3}$$

The selection of ω_{res} involves a trade-off between control interactions and filtering [15]. For active damping, typical values at which the capacitor voltage feedback is more effective are in the range $[0.1\omega_s, 0.2\omega_s]$ [15]. In this work, a transformer has not been employed in the experiments. A grid simulator is employed to form the low voltage ac grid, and physical inductances set the per-branch L_g values.

III. Proposed Approach

By inspection of Fig. 1, $Y_c(\omega)$ is the admittance defined by the converter side inductor and the closed loop controller actions (say from $\omega_s/6$ and beyond) [9], [20]. Due to system delays, $Y_c(\omega)$ tends to become non-passive at high frequencies, which in principle compromises the passivity compliance [9].

However, the key observation is that the input-admittance of the whole LCL grid-connected converter is the one defined as $Y_g(\omega)$ in Fig. 1, which is given by

$$Y_g(\omega) = \frac{1}{j\omega L_g + R_g} /\!/ \underbrace{[Y_p(\omega) + Y_c(\omega)]}_{Y_i(\omega) \equiv \text{inner-admittance}} \tag{4}$$

with

$$Y_p(\omega) = \frac{j\omega C}{j\omega C R_d + 1} = \frac{\omega^2 C^2 R_d + j\omega C}{1 + \omega^2 C^2 R_d^2} \tag{5}$$

being the admittance defined by the capacitor branch. The inner-admittance $Y_i(\omega)$ is defined as the sum of $Y_c(\omega)$ and $Y_p(\omega)$. As said, $Y_c(\omega)$ tends to become non-passive in the high frequency range. However, as $|Y_p(\omega)|$ also increases with frequency, the assumptions $|Y_p(\omega)| >> |Y_c(\omega)|$, and hence, $Y_i(\omega) \approx Y_p(\omega)$ become reasonable for frequencies well above ω_{res}.

The physical meaning and its implications on passivity and stability are clear: the high frequency components in the grid side mainly flow through the capacitor branch and hardly reach $i_c(t)$ closed-loop; therefore, the control actions derived from the disturbance are negligible to cause positive feedback or instability. Design guidelines to shape $Y_g(\omega)$ passive in the high frequency range are given next.

A. Guidelines for Controller Tuning

A z-domain approach is considered to shape the converter admittance. $Y_c(z)$ is defined as a closed loop transfer function that relates the current through L_c, say $i_c(z)$, with $E_c(z)$ assumed to be an ideal voltage source [i.e., for modelling purposes $E_c(z)$ is considered a pure disturbance of the current controller] [10]. The whole system delay is accurately modelled by a unit delay added to an extra half sample due to PWM/ZOH operation [9], [10], [21], [24]. The z-domain expression is obtained by considering the sample and hold effects in the discretization of the plant: the control paths that drive into the discrete device are discretized by ZOH method, meanwhile the Tustin method is accurate to represent the dynamics only due to the disturbance [10], [21], [22], [24], [25].

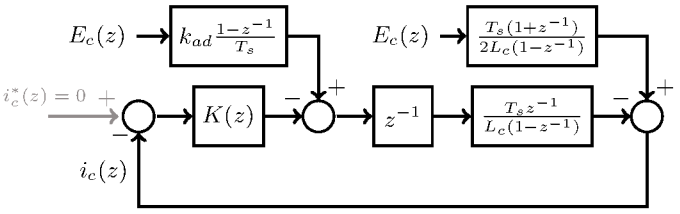

Fig. 2. Z-domain model of the current controller.

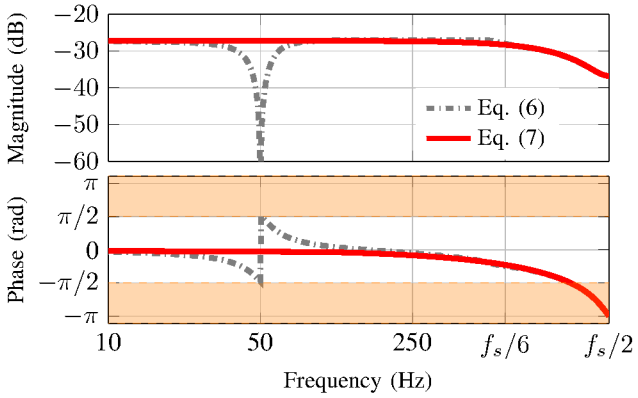

Fig. 3. Resonant controller influence on $Y_c(\omega)$.

Fig. 2 represents the disturbance to signal model employed to derive $Y_c(z)$, which gives

$$Y_c(z) = \frac{i_c(z)}{E_c(z)} = \frac{0.5z^3 + 0.5z^2 - k_{ad}/T_s z + k_{ad}/T_s}{z[L_{cs}/T_s z^2 - L_{cs}/T_s z + K(z)]}. \tag{6}$$

1) Calculation of k_{ad} and k_p: The resonant part is negligible at frequencies not in the vicinity of ω_1. In practice this covers the spectrum at which passivity compliance is studied. Fig. 3 shows the influence of the resonant regulator on the converter admittance. It can be seen that for passivity-based tuning purposes, the resonant filter in Fig. 1 can be neglected, so assuming $K(z) \approx k_p$ in the range of frequencies of interest, a simpler expression is obtained

$$Y_c(z) = \frac{i_c(z)}{E_c(z)} = \frac{0.5z^3 + 0.5z^2 - k_{ad}/T_s z + k_{ad}/T_s}{z(L_c/T_s z^2 - L_c/T_s z + k_p)}. \tag{7}$$

This expression is of third order and bi-proper, with zeros and poles depending on k_{ad} and k_p, respectively. A convenient

This article has been accepted for publication in a future issue of this journal, but has not been fully edited. Content may change prior to final publication. Citation information: DOI 10.1109/TIE.2018.2835374, IEEE Transactions on Industrial Electronics

combination of k_{ad} and k_p produces a double zero-pole cancellation and reduces $Y_c(z)$ to a first order expression, i.e.,

$$Y_c(z) = \frac{(az+b)}{z}\frac{(L_c/T_s z^2 - L_{cs}/T_s z + k_p)}{(L_c/T_s z^2 - L_c/T_s z + k_p)}. \quad (8)$$

This order reduction is obtained with

$$k_{ad} = \frac{2T_s}{3} \quad \text{and} \quad k_p = \frac{2L_c}{3T_s} \quad (9)$$

giving rise to

$$Y_c(z) = \frac{1}{2L_c f_s}\frac{z+2}{z} = \frac{\pi}{L_c\omega_s}\frac{z+2}{z}. \quad (10)$$

The order reduction enhances the passivity as it reduces the phase variations in the $Y_c(z)$ frequency response [i.e., phase variations associated to poles and zeros at the region of interest]. However, this expression is a non-minimum phase that has a zero at -2. This zero is modeling the effect of delay and introduces more and more phase-delay as the frequency increases [26], [27]. The frequency domain response is analytically obtained by $Y_c(\omega) \equiv Y_c(z = e^{j\omega T_s})$. It can be observed that, despite being a first order expression, the phase delay reaches -180 deg at the Nyquist frequency. The critical frequency at which $Y_c(\omega)$ turns to be not passive is $\omega_s/3$.

2) Calculation of k_i: In principle, a fast transient response of the system is achieved with a relative high k_i [8], [21], [24]. However, as previously discussed, the resonant gain should be small enough so it does re-shape $Y_c(\omega)$ at frequencies very different from ω_1. In order to find a good trade-off, a flexible design rule is reported in [8], from which

$$0.1 \leq \frac{\sqrt{k_i L_c}}{k_p} \leq 0.5 \quad (11)$$

is a reasonable range for k_i. In principle, this rule provides enough flexibility in order to find a good trade-off between transient response and passivity compliance, as shown in the experimental results.

B. A Conservative Criterion for R_d Selection

Addition of R_d is a standard passive damping method, which aims to attenuate the peak of the LCL filter resonance [16]–[18]. The main drawback of this approach is due to the R_d dissipation losses, which eventually reduce the overall converter efficiency [16]–[18]. From the point of view of design, the effect of R_d in the stability of the system can be studied by the frequency response of the input-admittance. Clearly, the overall objective is to fulfill with the passivity criteria with a minimum value of R_d.

The input-admittance $Y_g(\omega)$, defined as in (4), can be also evaluated in the frequency domain [$Y_c(\omega) = Y_c(z = e^{j\omega T_s})$.] A conservative design to keep $Y_g(\omega)$ passive is given by $\mathrm{Re}\{Y_p(\omega)\} > -\mathrm{Re}\{Y_c(\omega)\}$ in the high frequency range (cf. Fig. 4). Since $\mathrm{Re}\{Y_p(\omega)\}$ is monotonically increasing, and $-\mathrm{Re}\{Y_c(\omega)\}$ reaches its maximum at $\omega_s/2$, a sufficient condition is obtained by $\mathrm{Re}\{Y_p(\omega_s/3)\} = -\mathrm{Re}\{Y_c(\omega_s/2)\}$, giving rise to the design rule

$$R_d \geq \frac{9\pi}{L_c C^2 \omega_s^3}. \quad (12)$$

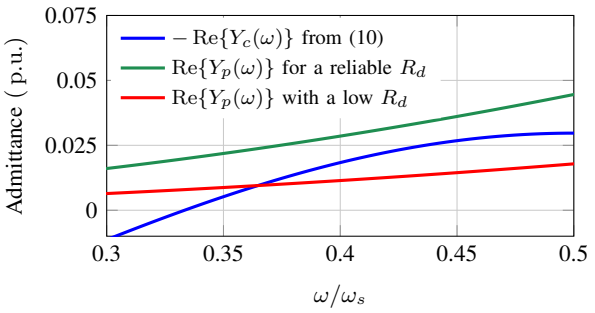

Fig. 4. R_d influence in $Y_g(\omega)$ passivity at the high-frequency region.

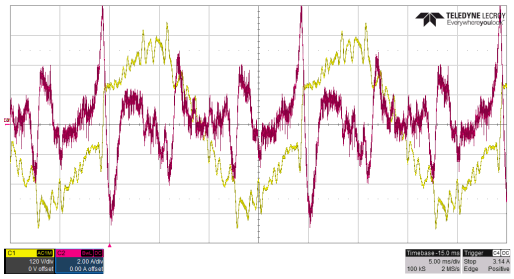

Fig. 5. A voltage harmonics signature programmed for admittance measurement: phase-A line-to-neutral voltage (yellow, source of perturbation) and phase-A grid current (red, response to the perturbation).

1) Effect of Natural Damping: It should be pointed out that the use of (12) as a design rule is provided for a relative high power industrial equipment working at rated conditions, where non-linear dissipation effects (e.g., copper and iron losses in magnetics due to switching harmonics [15], [28]) are negligible. However, an experimental verification in a low-scale experimental set-up would be meaningless since, as already reported in previous works such as [15], [20], [29], [30], there is a significant dissipation reflected as a high apparent R_c value [28]–[30]. E.g., taking representative values from [30], which analyzes a similar test-bench as the one employed in this work, R_c would be in the order of a few Ω; however, using the values of our test-bench, (12) gives a value lower than $1\,\Omega$ as a conservative one for R_d. Clearly, the lab-scale system already has a high natural passive damping, which drastically improves the closed loop dynamics without needing much further action. For example, the effect of adding/removing an external R_d resistor in our experiment has been found negligible in practice.

IV. Experimental Verification

The system described in Fig. 1 is replicated in a low scale lab prototype. The converter hardware is based on a low power industrial drive by *Danfoss*. The control is implemented in a rapid prototype target *dSpace D1006*. The grid is given by a *Chroma 61845* grid-simulator, which allows to program harmonics up to the 50^{th} component (cf. Fig. 5). The physical parameters of the test-bed are shown in Table I. For the sake of generality, two different sampling frequencies have been considered; i.e., different resonance over sampling frequency ratios. For the given power ratings, the LCL filter resonance

This article has been accepted for publication in a future issue of this journal, but has not been fully edited. Content may change prior to final publication. Citation information: DOI 10.1109/TIE.2018.2835374, IEEE Transactions on Industrial Electronics

TABLE I
PHYSICAL SYSTEM PARAMETERS

Circuit Parameters	
Rated Power	$S = 2.5\,\text{kVA}$
Rated Voltage (Line to line RMS)	$V = 230\,\text{V}$
Converter inductance	$L_c = 8.6\,\text{mH}$
Converter equivalent resistance	$R_c \approx 2\,\Omega$ (cf. [30])
Capacitor	$C = 27\,\text{uF}$
Passive damping (ESR from C)	$R_d = 3m\,\Omega$
Grid Side Inductance	$L_g = 8.6\,\text{mH}$
Grid Side Resistor	$R_g = 0.27\,\Omega$
Resonance frequency	$f_{\text{res}} = 467\,\text{Hz}$
Test-bench scenario 1	
Switching/Sampling frequency	$f_{sw} = f_s = 4\,\text{kHz}$
Proportional gain	$k_p = 22.93\,\Omega$
Resonant gain	$k_i = 2800\,\Omega/\text{s}$
Active damping gain	$k_{ad} = 167e^{-6}\,\text{s}$
Test-bench scenario 2	
Switching/Sampling frequency	$f_{sw} = f_s = 3\,\text{kHz}$
Proportional gain	$k_p = 17.20\,\Omega$
Resonant gain	$k_i = 2400\,\Omega/\text{s}$
Active damping gain	$k_{ad} = 222e^{-6}\,\text{s}$

frequency and the sampling/switching frequencies have been selected low in order to take advantage of the grid simulator harmonic injection capability, which, for the selected sampling/switching frequencies, allows the admittances measurement beyond $\omega_s/2$.

Before representation and discussion of frequency domain curves, basic operation tests obtained with the converter design provided in section III-A are depicted in Figs. 6 and 7. For both test-cases, the current step (from 0 to 100% nominal current) responses and the responses to grid faults (40% voltage sag) are quick and damped, which are in a good agreement with the expected responses form the theoretical analysis, and overall proves the robustness of the system. As expected, the test-case with higher switching frequency, shows a slightly better current step response, and lower current peak for the grid faults test. The grid fault tests are a good method to evaluate the converter admittance, since by definition, the converter admittance is the converter current response against voltage variations [i.e., $Y_c(z) = i_c(z)/E_c(z)$]. The lower current peaks obtained in Fig. 6(a) in comparison with Fig. 7(a) is expected by the higher k_p, since the disturbance rejection capability at low frequencies, mostly depends on k_p [$|Y_c(j\omega)| \approx 1/k_p,\ \forall\omega < \omega_c$, being ω_c the controller closed loop bandwidth] [20]. This can be appreciated in Figs. 8(a) and 8(c), where $|Y_c(j\omega \approx 0)|$ is -27.23 dB and -24.75 dB for values of k_p of 22.93 and 17.20, respectively.

Subsequently, $Y_c(\omega)$ and $Y_g(\omega)$ measurements in the frequency domain are provided. The procedure to measure $Y_c(\omega)$ and $Y_g(\omega)$ are inspired in the EN-50388 normative [7]: i) for each point, the voltage harmonic components are programmed at $E_c(t)$ or $E_g(t)$ and their Fast Fourier Transform (FFT) are performed (magnitude and phase); ii) the converter control is activated with $i_c(t) = 0$ and its steady state is reached quickly; then the FFT for $i_c(t)$ or $i_g(t)$ (magnitude and phase) is also performed; iii) $Y_c(\omega)$ and $Y_g(\omega)$ are calculated as

$$Y_{c,g}(\omega) = \frac{|i_{c,g}(\omega)|^{\text{FFT}}}{|E_{c,g}(\omega)|^{\text{FFT}}}[\angle\phi^{\text{FFT}}_{i_{c,g}(\omega)} - \angle\phi^{\text{FFT}}_{E_{c,g}(\omega)}] \tag{13}$$

with the FFT superscript referring to data obtained by spectral analysis. As an example of the procedure, Fig. 5 shows time domain responses of the input phase voltage waveform with the programmed harmonic components, more specifically with the 5-7-8-10-11-13-16-19-22-26-30-35-41-50th harmonic components, and the resultant $i_g(\omega)$ phase current.

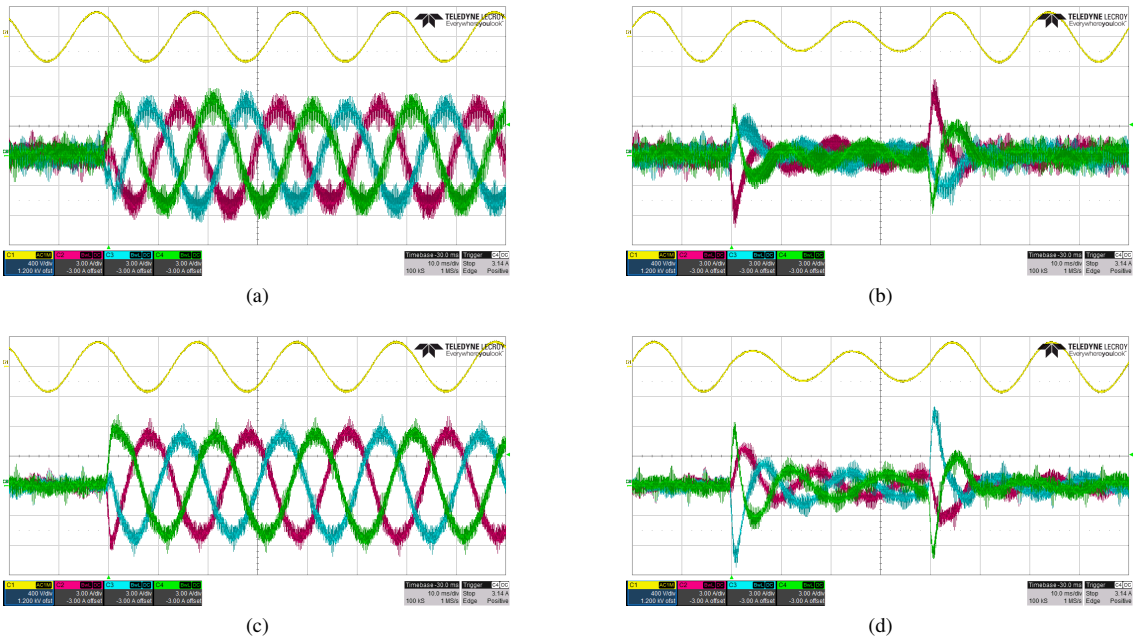

(a) (b) (c) (d)

Fig. 6. Reference tracking and disturbance rejection tests for the test-bench scenario 1. The yellow curve shows $E_c(t)$ in all the cases; $i_c(t)$ or $i_g(t)$ are shown depending on the test as described next. (a) $i_c(t)$ current command step; (b) $i_c(t)$ response to a voltage step (i.e., a grid fault) with $i_c^*(t) = 0$; (d) $i_g(t)$ for a current command step; (d) $i_g(t)$ response to a voltage step (i.e., a grid fault) with $i_c^*(t) = 0$.

This article has been accepted for publication in a future issue of this journal, but has not been fully edited. Content may change prior to final publication. Citation information: DOI 10.1109/TIE.2018.2835374, IEEE Transactions on Industrial Electronics

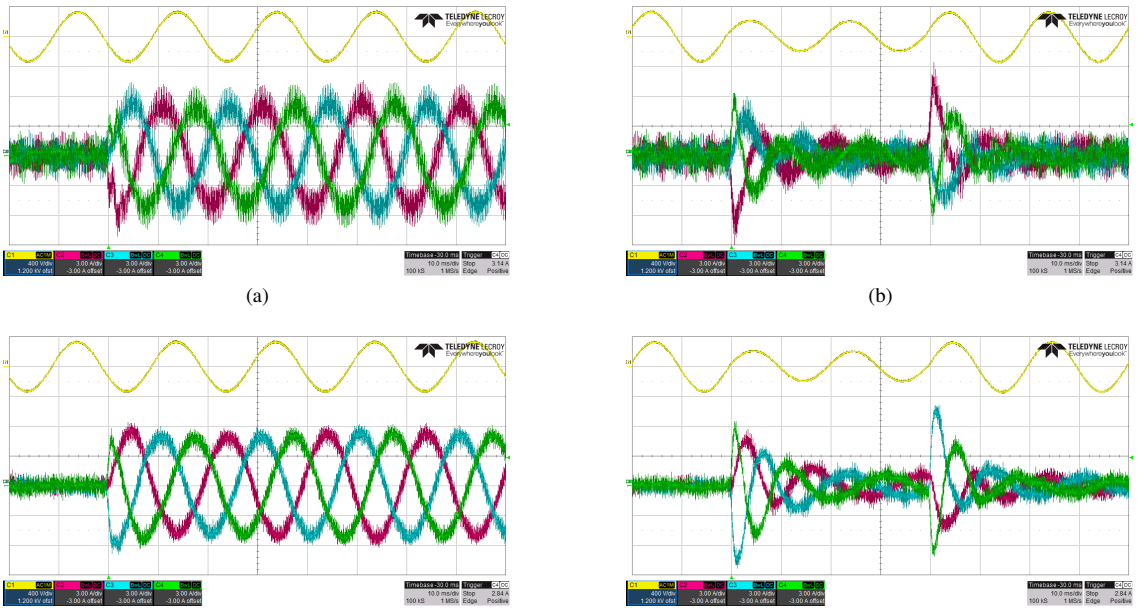

Fig. 7. Reference tracking and disturbance rejection tests for the test-bench scenario 2. The yellow curve shows $E_c(t)$ in all the cases; $i_c(t)$ or $i_g(t)$ are shown depending on the test as described next. (a) $i_c(t)$ current command step; (b) $i_c(t)$ response to a voltage step (i.e., a grid fault) with $i_c^*(t) = 0$; (d) $i_g(t)$ for a current command step; (d) $i_g(t)$ response to a voltage step (i.e., a grid fault) with $i_c^*(t) = 0$.

Fig. 8(a) shows $Y_c(\omega)$ measurements over the theoretical curve for the test-bench scenario 1 (cf. Table I). In the low frequency range (up to $\omega_s/6$ region), the measurements well match the theoretical expression given by (10). Passivity compliance in the $\omega_s/6$ region is achieved thanks to the effective active damping action [9]. At the high frequency range (well beyond $\omega_s/6$), $Y_c(\omega)$ also tends to comply with the passivity requirement, conversely to the theoretical expression. An explanation to this behaviour can be regarded to the high inherent passive damping of typical low-power lab-scale test-benches [15], [20], [29], [30] in combination with a negligible effectiveness of the control action as the frequencies approach the Nyquist limit [10], [13], [14]. Fig. 8(b) shows $Y_g(\omega)$ measurements for the test-bench scenario 1: passivity compliance is fully achieved in all the spectrum. Fig. 8(c) and Fig. 8(d) show the measurements for the test-bench scenario 2. Similar observations as in the test-bench scenario 1 are found: high parasitic damping and loss of effective control action are reflected in $Y_c(\omega)$; $Y_g(\omega)$ passivity compliance is achieved.

Overall, the results shown in Figs. 8 prove the validity of the approach, but it is also clear that the beneficial effect of damping that may ease to obtain passivity compliance. Presumably, a real scale system rated for a higher order of magnitude in power, the natural dissipation of the circuit is significantly smaller [30]. In order to evaluate the approach in more demanding scenarios, the current controller is artificially driven near unstable implementations; to do so, an extra delay is added as method to artificially impair[1] the $Y_c(\omega)$ shaping (cf. appendix). An accurate extra delay is added using all pass filters of the form

$$\mathbf{A}(z) = \frac{-z_0 + z^{-1}}{1 - z_0 z^{-1}}\mathbf{I}. \tag{14}$$

in series with the control action; by defining T_{ed} as the artificially added extra delay, the all pass-filter parameter is given by $z_0 = (1 - T_{\text{ed}}/T_s)/(1 + T_{\text{ed}}/T_s)$.

Fig. 9(a) shows $Y_c(\omega)$ curves detailed in a high-frequency region to show two main effects. For enough timed delay non-passive regions are obtained, first in the highest frequency region (as imposed by the grid-simulator), and for even bigger delay also in the $\omega_s/6$ region. Fig. 9(b) shows $Y_g(\omega)$ measurements for the cases in which the LCL system is stable, which also correspond to a $Y_g(\omega)$ passivity compliant. However, the whole LCL system was found unable to work when $Y_c(\omega)$ is not passive around the $\omega_s/6$ region (the grid-simulator issues an over-current alarm in such scenarios). The same behaviour is observed for the second tests case, for which figures of merit are depicted in Figs. 9(c) and 9(b).

Overall, the experimental verification clearly proves the main hypothesis of the work: the LCL filter naturally provides passivity in the high frequency region, where the control action naturally becomes ineffective. It can be also mentioned that, at the $\omega_s/6$ region, shaping $Y_c(\omega)$ for passivity is needed to effectively damp the LCL resonance.

V. Conclusions

This work addresses the input-admittance passivity compliance of LCL grid-connected VSCs. Design guidelines for the controller design are developed in the z-domain, with capacitor voltage based active damping used as degree of freedom. The role of passive resistors is also discussed. As a main

[1]Other methods to artificially impair the dynamics of damped LCL systems (e.g., for assessment of the k_{ad} tuning) are reported [15], [20].

This article has been accepted for publication in a future issue of this journal, but has not been fully edited. Content may change prior to final publication. Citation information: DOI 10.1109/TIE.2018.2835374, IEEE Transactions on Industrial Electronics

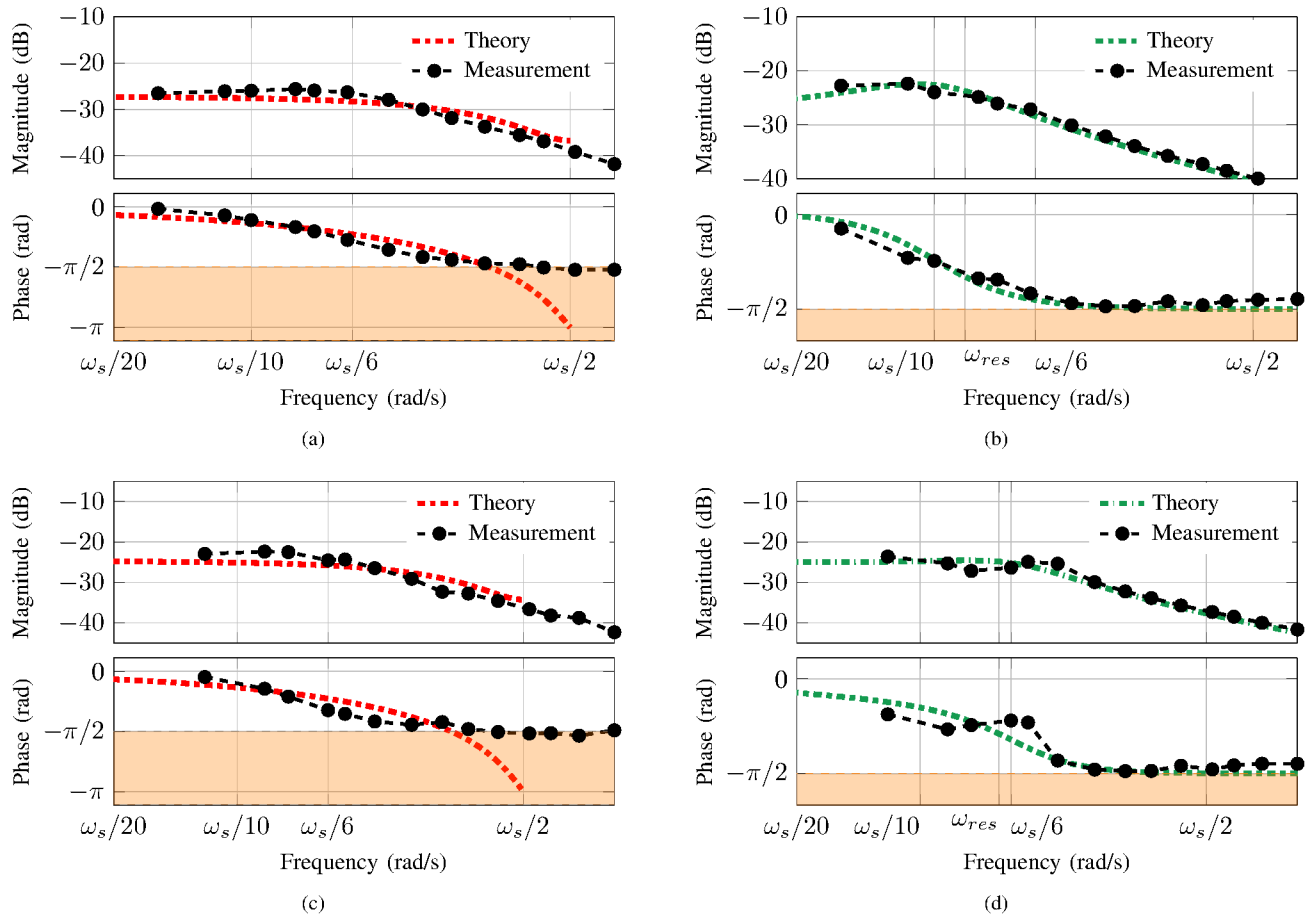

Fig. 8. $Y_c(\omega)$ and $Y_g(\omega)$ measurements for passivity compliance assessment. (a) $Y_c(\omega)$ for test-bench scenario 1. (b) $Y_g(\omega)$ for test-bench scenario 1.(c) $Y_c(\omega)$ for test-bench scenario 2. (d) $Y_g(\omega)$ for test-bench scenario 2.

hypothesis, it is stated that the LCL filter is a convenient structure because it helps to provide passivity in the high frequency range (well beyond $\omega_s/6$). A comprehensive set of experiments, including a high performance grid simulator, has been deployed. The experimental results prove how the LCL structure is convenient for input-admittance passivity compliance. The importance of shaping $Y_c(\omega)$ passive in the $\omega_s/6$ region has been also checked experimentally.

APPENDIX

This appendix provides a simplified analysis to show how the system delay compromises the passivity and countermeasures the natural damping of the system. For the sake of simplicity, a continuous-domain input-admittance without active damping and resonant controller is considered as follows

$$Y_c(j\omega) = \frac{1}{j\omega L_c + R_c + k_p e^{-j\omega T_d}} \tag{15}$$

with T_d being the system delay. In order to get the real part of $Y_c(j\omega)$, the numerator and denominator of (15) are multiplied by the complex conjugate of the denominator and the Euler formula is used to substitute complex exponential terms by sine/cosine functions. The resulting expression is

$$\text{Real}\{Y_2(\omega)\} = \frac{R_c + k_p\cos(T_d\omega)}{L_c^2\omega^2 + k_p^2 + R_c^2 - 2L_c\omega k_p\sin(T_d\omega) + 2R_c k_p\cos(T_d\omega)} \tag{16}$$

From basic property of complex numbers, the denominator of (16) is positive. Therefore, the passivity condition is achieved for the frequencies such that

$$R_c + k_p\cos(T_d\omega) \geq 0 \tag{17}$$

The critical frequency for passivity compliance is given by

$$\omega_{\text{crit}} = \frac{\text{acos}(-R_c/k_p)}{T_d} \tag{18}$$

From (18): i) ω_{crit} increases when R_c increases; ii) ω_{crit} decreases when T_d increases. Therefore, it is shown how the system delay is a countermeasure to the damping of the system. It may be noticed that if passive damping is neglected, i.e., $R_c \approx 0$, and also $T_d = 1.5/f_s$, then $\omega_{\text{crit}} = \omega_s/6$, which is in accordance to previous literature [9].

This article has been accepted for publication in a future issue of this journal, but has not been fully edited. Content may change prior to final publication. Citation information: DOI 10.1109/TIE.2018.2835374, IEEE Transactions on Industrial Electronics

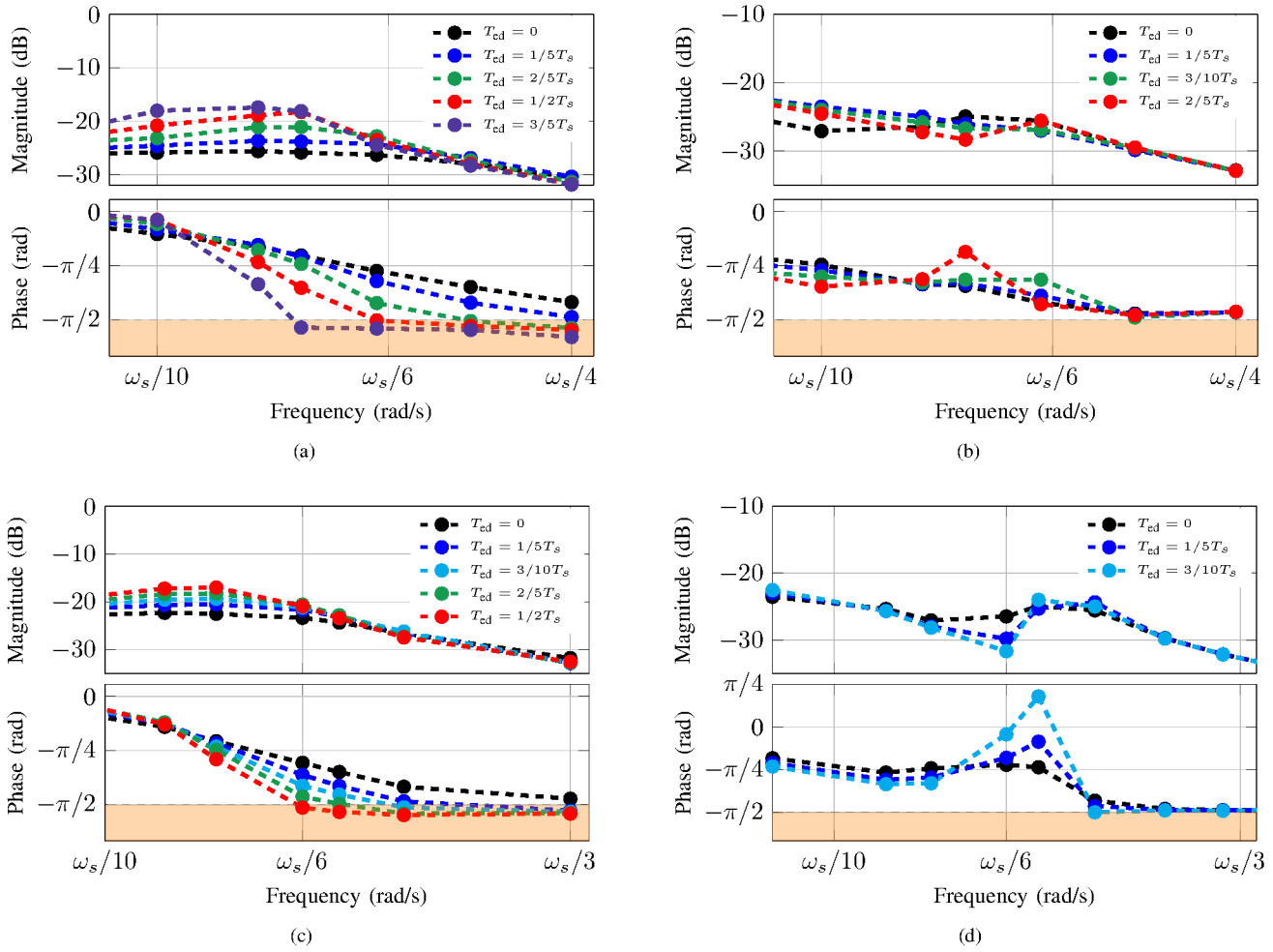

Fig. 9. $Y_c(\omega)$ and $Y_g(\omega)$ measurements for passivity compliance assessment with consideration of extra delays for more demanding conditions. (a) $Y_c(\omega)$ for test-bench scenario 1. (b) $Y_g(\omega)$ for test-bench scenario 1.(c) $Y_c(\omega)$ for test-bench scenario 2. (d) $Y_g(\omega)$ for test-bench scenario 2.

REFERENCES

[1] E. Mollerstedt and B. Bernhardsson, "Out of control because of harmonics-an analysis of the harmonic response of an inverter locomotive," *IEEE Control Syst. Mag.*, vol. 20, no. 4, pp. 70–81, 2000.

[2] D. Dujic et al., "Power electronic traction transformer-low voltage prototype," *IEEE Trans. Power Electron.*, vol. 28, no. 12, pp. 5522–5534, 2013.

[3] M. Bradt et al., "Harmonics and resonance issues in wind power plants," in *Proc. of the IEEE PES GM*, 2011.

[4] H. Kocewiak, J. Hjerrild, and C. Bak, "Wind turbine converter control interaction with complex wind farm systems," *IET Renewable Power Generation*, vol. 7, no. 4, pp. 380–389, 2013.

[5] L. Sainz et al., "Effect of wind turbine converter control on wind power plant harmonic response and resonances," *IET Electric Power App.*, 2017.

[6] J. E. Colgate and N. Hogan, "Robust control of dynamically interacting systems," *International J. of Control*, vol. 48, no. 1, pp. 65–88, 1988.

[7] *EN50388. Railway Applications – Power supply and rolling stock – Technical criteria for the coordination between power supply (substation) and rolling stock to achieve interoperability*, Cenelec Std., 2012.

[8] L. Harnefors, L. Zhang, and M. Bongiorno, "Frequency-domain passivity-based current controller design," *IET Power Electron.*, vol. 1, no. 4, pp. 455–465, Dec. 2008.

[9] L. Harnefors, A. G. Yepes, A. Vidal, and J. Doval-Gandoy, "Passivity-based controller design of grid-connected vscs for prevention of electrical resonance instability," *IEEE Trans. Ind. Electron.*, vol. 62, no. 2, pp. 702–710, 2015.

[10] F. D. Freijedo, D. Dujic, and J. A. Marrero-Sosa, "Design for passivity in the z-domain for LCL grid-connected converters," in *Proc. of the IEEE Industrial Electronics Society Annual Conference*, pp. 7016–7021, Firenze, Italy, Oct. 2016.

[11] H. Bai, X. Wang, and F. Blaabjerg, "Passivity enhancement in res based power plant with paralleled grid-connected inverter," *IEEE Trans. Ind. Appl.*, vol. 53, no. 4, pp. 3793 – 3802, 2017.

[12] L. Harnefors, R. Finger, X. Wang, H. Bai, and F. Blaabjerg, "Vsc input-admittance modeling and analysis above the Nyquist frequency for passivity-based stability assessment," *IEEE Trans. Ind. Electron.*, vol. 64, no. 8, pp. 6362–6370, Aug. 2017.

[13] C. M. Wolf, M. W. Degner, and F. Briz, "Analysis of current sampling errors in pwm vsi drives," *IEEE Trans. Ind. Appl.*, vol. 51, no. 2, pp. 1551–1560, 2015.

[14] K. Sozanski, *Digital Signal Processing in Power Electronics Control Circuits*. Springer Verlag, 2013.

[15] J. Dannehl, F. Fuchs, S. Hansen, and P. Thogersen, "Investigation of active damping approaches for pi-based current control of grid-connected pulse width modulation converters with LCL filters," *IEEE Trans. Ind. Appl.*, vol. 46, no. 4, pp. 1509–1517, 2010.

[16] R. Pena-Alzola et al., "Analysis of the passive damping losses in LCL-filter-based grid converters," *IEEE Trans. Power Electron.*, vol. 28, no. 6, pp. 2642–2646, 2013.

[17] A. Rockhill, M. Liserre, R. Teodorescu, and P. Rodriguez, "Grid-filter design for a multimegawatt medium-voltage voltage-source inverter," *IEEE Trans. Ind. Electron.*, vol. 58, no. 4, pp. 1205–1217, 2011.

[18] M. Liserre, F. Blaabjerg, and S. Hansen, "Design and control of an LCL-filter-based three-phase active rectifier," *IEEE Transactions on Industry*

Applications, vol. 41, no. 5, pp. 1281–1291, sept.-oct. 2005.

[19] G. Gohil, L. Bede, R. Teodorescu, T. Kerekes, and F. Blaabjerg, "Line filter design of parallel interleaved vscs for high-power wind energy conversion systems," *IEEE Trans. Power Electron.*, vol. 30, no. 12, pp. 6775–6790, 2015.

[20] F. D. Freijedo et al., "A Root-Locus Design Methodology Derived from the Impedance/Admittance Stability Formulation and Its Application for LCL Grid-Connected Converters in Wind Turbines," *IEEE Trans. Power Electron.*, vol. 32, no.10, pp. 8218 – 8228, 2017.

[21] A. Vidal et al., "Transient response evaluation of stationary-frame resonant current controllers for grid-connected applications," *IET Power Electronics*, vol. 7, no. 7, pp. 1714–1724, 2014.

[22] G. C. Goodwin, S. F. Graebe, and M. E. Salgado, *Control System Design*. Prentice Hall, 2000.

[23] *IEC 61400-21 Ed.2, Wind turbines – Part 21: Measurement and assessment of power quality characteristics of grid connected wind turbines*, IEC Std., Aug. 2008.

[24] A. Vidal et al. "Assessment and optimization of the transient response of proportional-resonant current controllers for distributed power generation systems," *IEEE Trans. Ind. Electron.*, vol. 60, no. 4, pp. 1367–1383, Apr. 2013.

[25] G. F. Franklin, J. D. Powell, and M. L. Workman., *Digital Control of Dynamic Systems (3rd Edition)*, ., Ed. Addison-Wesley, 1997.

[26] K. J. Astrom, P. Hagander, and J. Sternby, "Zeros of sampled systems," in *Proc. 19th IEEE Conf. Decision and Control including the Symp. Adaptive Processes*, pp. 1077–1081, Dec. 1980.

[27] J. Hoagg and D. Bernstein, "Nonminimum-phase zeros - much to do about nothing - classical control - revisited part II," *IEEE Control Syst. Mag.*, vol. 27, no. 3, pp. 45–57, Jun. 2007.

[28] P. W. Lehn, "Exact modeling of the voltage source converter," *IEEE Trans. Power Del.*, vol. 17, no. 1, pp. 217–222, Jan. 2002.

[29] A. Vidal et al. "A technique to estimate the equivalent loss resistance of grid-tied converters for current control analysis and design," *IEEE Trans. Power Electron.*, vol. 30, no. 3, pp. 1747–1761, 2015.

[30] A. Vidal et al. "A method for identification of the equivalent inductance and resistance in the plant model of current-controlled grid-tied converters," *IEEE Trans. Power Electron.*, vol. 30, no. 12, pp. 7245–7261, 2015.

Enrique Rodriguez-Diaz (S'15-M'18) received the B.Sc. and Msc degrees in Electronics Engineering at the University of Oviedo, Oviedo, Spain, in 2012 and 2014,respectively. He obtained his PhD degree in Power Electronics from Aalborg Universitet, Denmark, in 2018, where currently is a Postdoctoral Researcher. In 2017, he was a guest researcher at the Power Electronic Laboratory at EPFL. He is a member of the International Electrotechnical Commission System Evaluation Group SEG4 on Low Voltage DC Applications, Distribution, and Safety for Use in Developed and Developing Economies. His research interests include DC distribution systems, control of power converters and microgrids.

Francisco D. Freijedo (M'07-SM'16) received the M.Sc. degree in physics from the University of Santiago de Compostela, Santiago de Compostela, Spain, in 2002 and the Ph.D. degree in Electrical Engineering from the University of Vigo, Vigo, Spain, in 2009. From 2005 to 2011, he was a Lecturer in the Department of Electronics Technology, University of Vigo. From 2011 to 2014, he worked in Gamesa Innovation and Technology as a Power Electronics Control Engineer, where he was involved in Wind Energy projects. From 2014 to 2016, he was a Postdoctoral Researcher in the Department of Energy Technology, Aalborg University. Since 2016, he is a Scientific Collaborator of the Power Electronics Laboratory, Ecole Polytechnique Federale de Lausanne. His research interests include many power conversion technologies and challenging control problems.

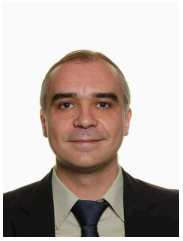

Josep M. Guerrero (S'01-M'04-SM'08-F'15) received the B.S. degree in telecommunications engineering, the M.S. degree in electronics engineering, and the Ph.D. degree in power electronics from the Technical University of Catalonia, Barcelona, in 1997, 2000 and 2003, respectively. Since 2011, he has been a Full Professor with the Department of Energy Technology, Aalborg University, Denmark, where he is responsible for the Microgrid Research Program. From 2012 he is a guest Professor at the Chinese Academy of Science and the Nanjing University of Aeronautics and Astronautics; and from 2014 he is chair Professor in Shandong University. His research interests is oriented to different microgrid aspects, including power electronics, distributed energy-storage systems, hierarchical and cooperative control, energy management systems, and optimization of microgrids and islanded minigrids. In 2014 he was awarded by Thomson Reuters as ISI Highly Cited Researcher, and in 2015 same year he was elevated as IEEE Fellow for contributions to "distributed power systems and microgrids".

Juan-Alberto Marrero-Sosa received the B.S. and M.Sc. degrees in Electrical Engineering, and in Control and Electronics Engineering from the University Carlos III of Madrid, Madrid, Spain in 2002, 2005 and 2005 respectively. Since then he has worked as development engineer of power electronics converters for several international companies, mainly in the sectors of renewable energy and railways. Since 2012 he has been working for ABB in the Development Department for Medium Voltage Drives and Traction Converters in Turgi, Switzerland. His research interests include power electronics, renewable energy and advanced control techniques.

Drazen Dujic (S'03-M'09-SM'12) received the Dipl.-Ing. and M.Sc. degrees from the University of Novi Sad, Novi Sad, Serbia, in 2002 and 2005, respectively, and the Ph.D. degree from Liverpool John Moores University, Liverpool, U.K., in 2008, all in Electrical Engineering. From 2002 to 2006, he was a Research Assistant with the Department of Electrical Engineering, University of Novi Sad. From 2006 to 2009, he was a Research Associate with Liverpool John Moores University. From 2009 to 2013, he was with the ABB Corporate Research Center, Switzerland, as a Principal Scientist working on Power Electronics Projects. During 2010-2011, he was involved in the development of the Power Electronic Traction Transformer (PETT). From 2013 to 2014, he was with ABB Medium Voltage Drives, Turgi, Switzerland, as an R&D Platform Manager. He is currently an Assistant Professor with the Ecole Polytechnique Federale de Lausanne, Lausanne, Switzerland, where he is also the Director of the Power Electronics Laboratory. He has authored more than 100 scientific publications and has filed 11 patents. His current research interests include design of advanced high-power electronics systems and high-performance drives. Dr. Dujic is an Associate Editor for the IEEE TRANSACTIONS ON INDUSTRIAL ELECTRONICS, IEEE TRANSACTIONS ON POWER ELECTRONICS, and IET Electric Power Applications. He received the First Prize Paper Award from the Electrical Machines Committee of the IEEE IES at IECON 2007. In 2014, he received the Isao Takahashi Power Electronics Award for outstanding achievement in Power Electronics.